Structure, Volume *21*

Supplemental Information

Structure, Dynamics, Evolution, and Function of a Major Scaffold Component in the Nuclear Pore Complex

Parthasarathy Sampathkumar, Seung Joong Kim, Paula Upla, William J. Rice, Jeremy Phillips, Benjamin L. Timney, Ursula Pieper, Jeffrey B. Bonanno, Javier Fernandez-Martinez, Zhanna Hakhverdyan, Natalia E. Ketaren, Tsutomu Matsui, Thomas M. Weiss, David L. Stokes, J. Michael Sauder, Stephen K. Burley, Andrej Sali, Michael P. Rout, and Steven C. Almo

Inventory of Supplemental Information

Supplemental Experimental Procedures
Detailed Experimental Procedures

Supplemental References

Supplementary Figure S1, Sampathkumar et al.,

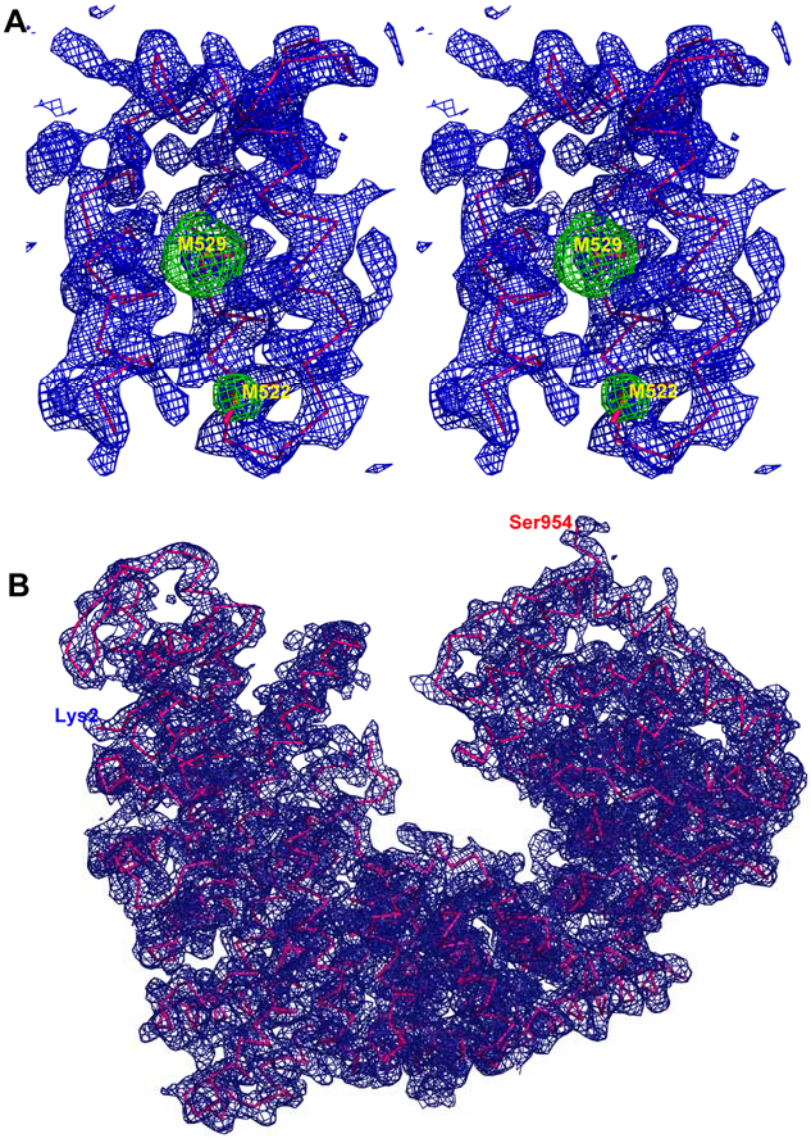

Figure S1, related to Figure 1. **Electron density maps of ScNup192(2-960).**

(A) Final mFo-DFc omit electron density map for a representative region of ScNup192(2-960) comprising residues Ala476 to Ala540 in blue displayed at 1.8 σ. Anomalous difference map obtained with final calculated phases shown in green for Se-Met522 (bottom) and Se-Met529 (middle) at 10.0 σ.

(B) The 2mFo-DFc electron density map for the entire length of ScNup192(2-960) at the end of the refinement displayed at 1.0σ in blue. Molecular backbone is represented as ribbon with carbons in magenta.

Supplementary Figure S2, Sampathkumar et al.,

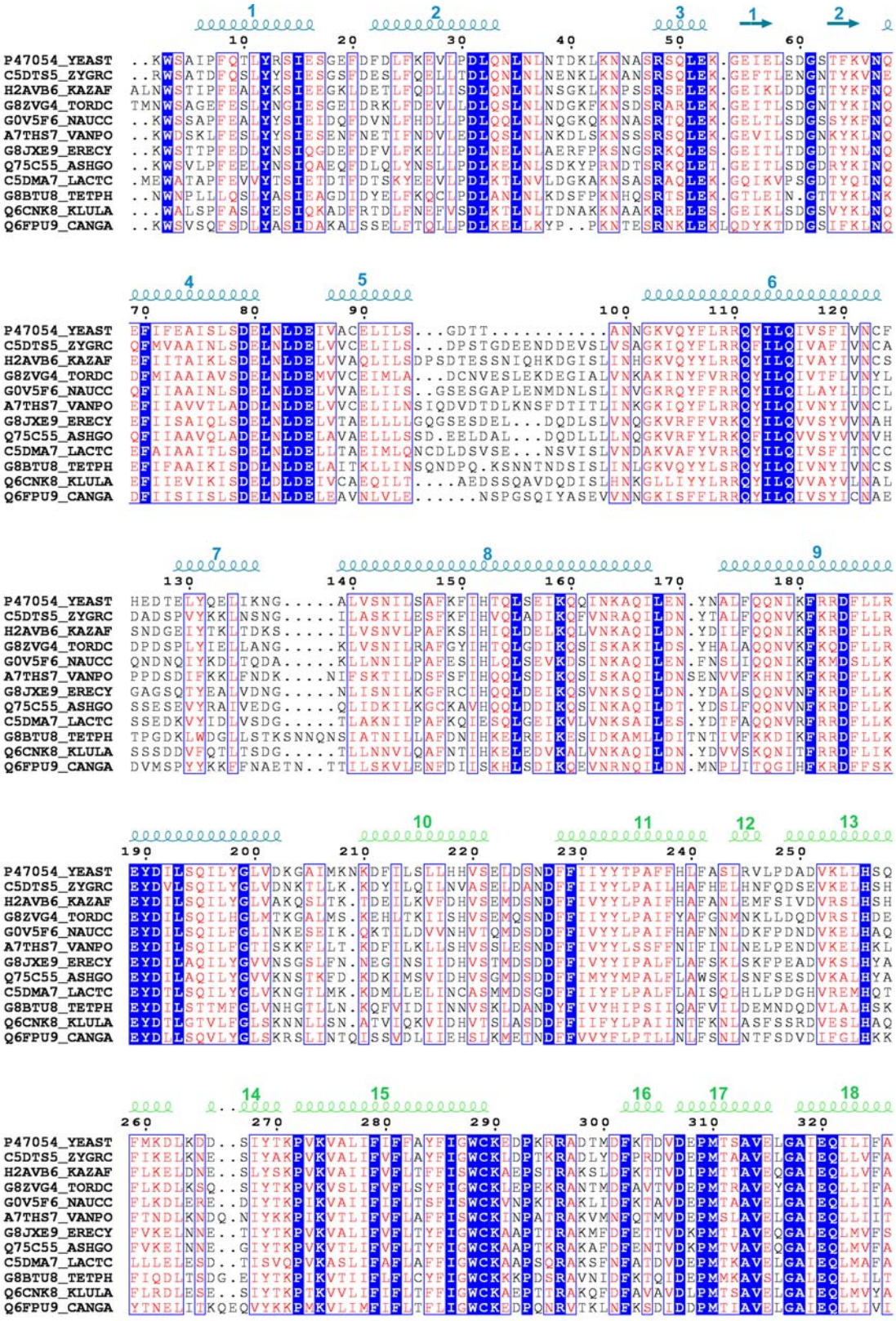

Supplementary Figure S2, Sampathkumar et al.,

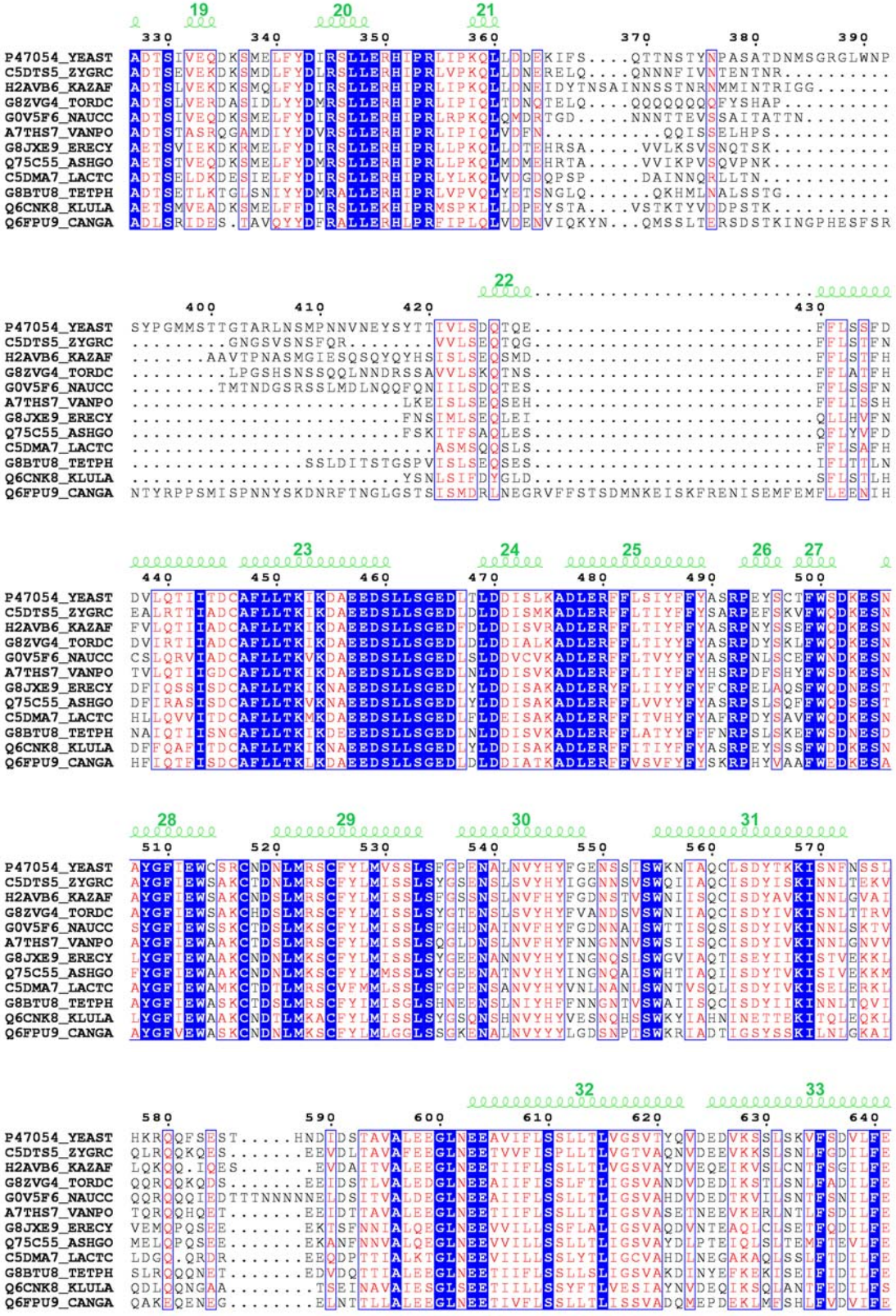

Supplementary Figure S2, Sampathkumar et al.,

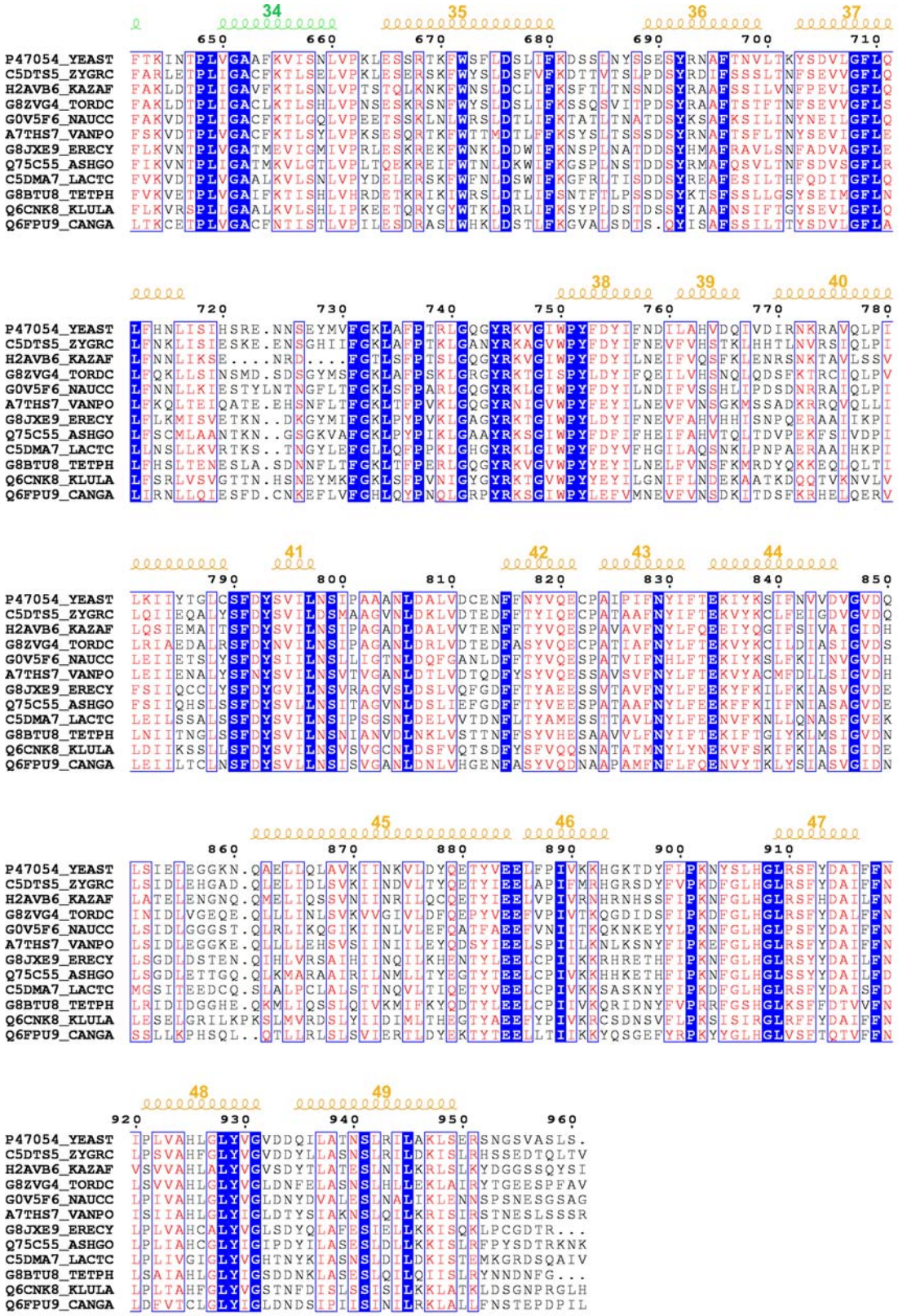

Figure S2, related to Figure 1. Conservation of Nup192(2-960) sequences.

Sequence alignment of ScNup192(2-960) with corresponding sequence-range from 11 other Nup192 of yeast / fungal origin labeled with respective uniprot entry names (www.uniprot.org). Conserved residues are shown in blue. Secondary structure elements are shown at the top with D1, D2, and D3 domain in cyan, green, and gold, respectively. Sequence alignment was performed using ClustalW (Larkin et al., 2007; http://www.ebi.ac.uk/Tools/msa/clustalw2/) and the illustration was prepared with ESPript (Gouet et al., 2003; http://espript.ibcp.fr/ESPript/cgi-bin/ESPript.cgi).

Supplementary Figure S3, Sampathkumar et al.,

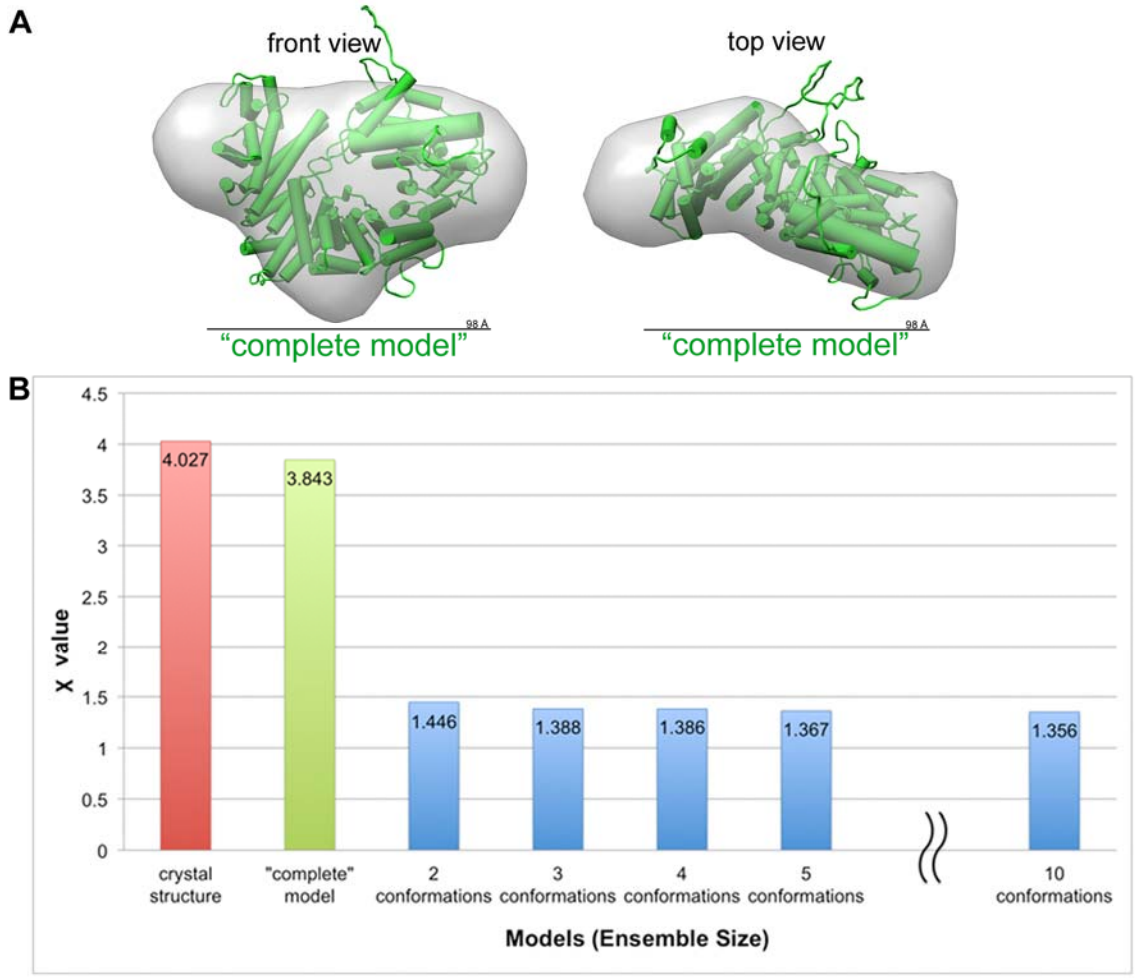

Figure S3, related to Figure 2. Conformational sampling analysis to reproduce the experimental SAXS profile

(A) Fit of the MODELLER derived "complete model" of ScNup192(2-960) to its *ab initio* SAXS shape in solution

(B) Comparison of the χ values (fit to the experimental SAXS profile) computed from the crystal structure, the "complete" model, and various sizes of ensemble of conformations (2 to 10 conformations). The χ values barely changes with larger sizes of ensemble. Thus, the ensemble of two conformations is sufficient to explain the experimental SAXS profile.

Supplementary Figure S4, Sampathkumar et al.,

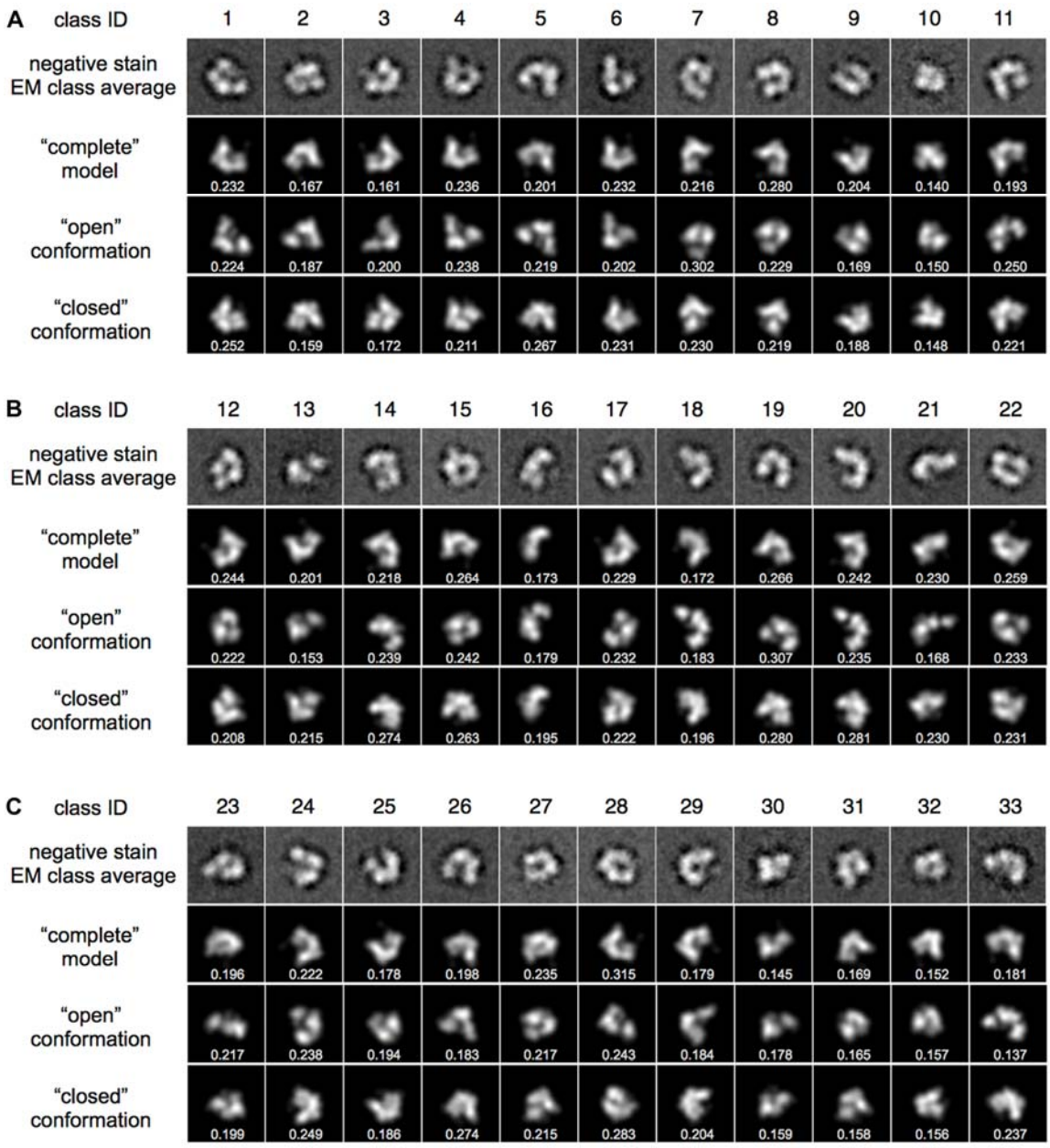

Supplementary Figure S4, Sampathkumar et al.,

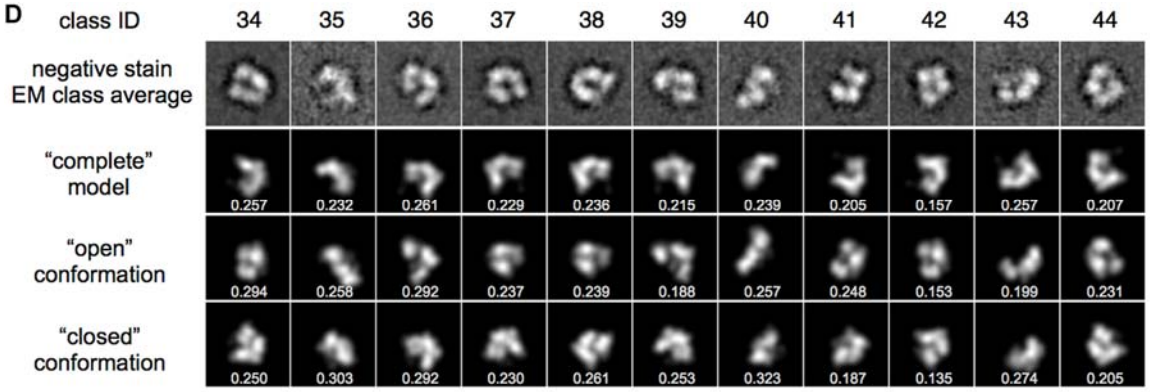

Figure S4 related to Figure 2. **EM class averages and projections of ScNup192(2-960).**

(A-D) The top row in each panels shows negative stain EM class averages from iterative stable alignment and clustering (ISAC) of 4,580 particles. After 7 generations, 3824 particles accounted for 44 classes. The number of particles comprising each class is indicated. Scale bar, 5 nm. Subsequent rows in each panel show projections of the "complete model", "open" conformation, and "closed" conformation of ScNup192(2-960). The *em2D* score (shown in the bottom of each projection) is defined as "one minus the cross-correlation coefficient between the image and the optimal model projection (1-ccc)", measuring the minimal difference between the image and a model projection. The projections and the *em2D* scores of the models are computed using *EMageFit* application of the Integrated Modeling Platform (IMP) package. In conclusion, the 44 class averages are not explained by any of a single-conformation alone, indicating heterogeneity of the ScNup192(2-960) on the EM grid.

Supplementary Figure S5, Sampathkumar et al.,

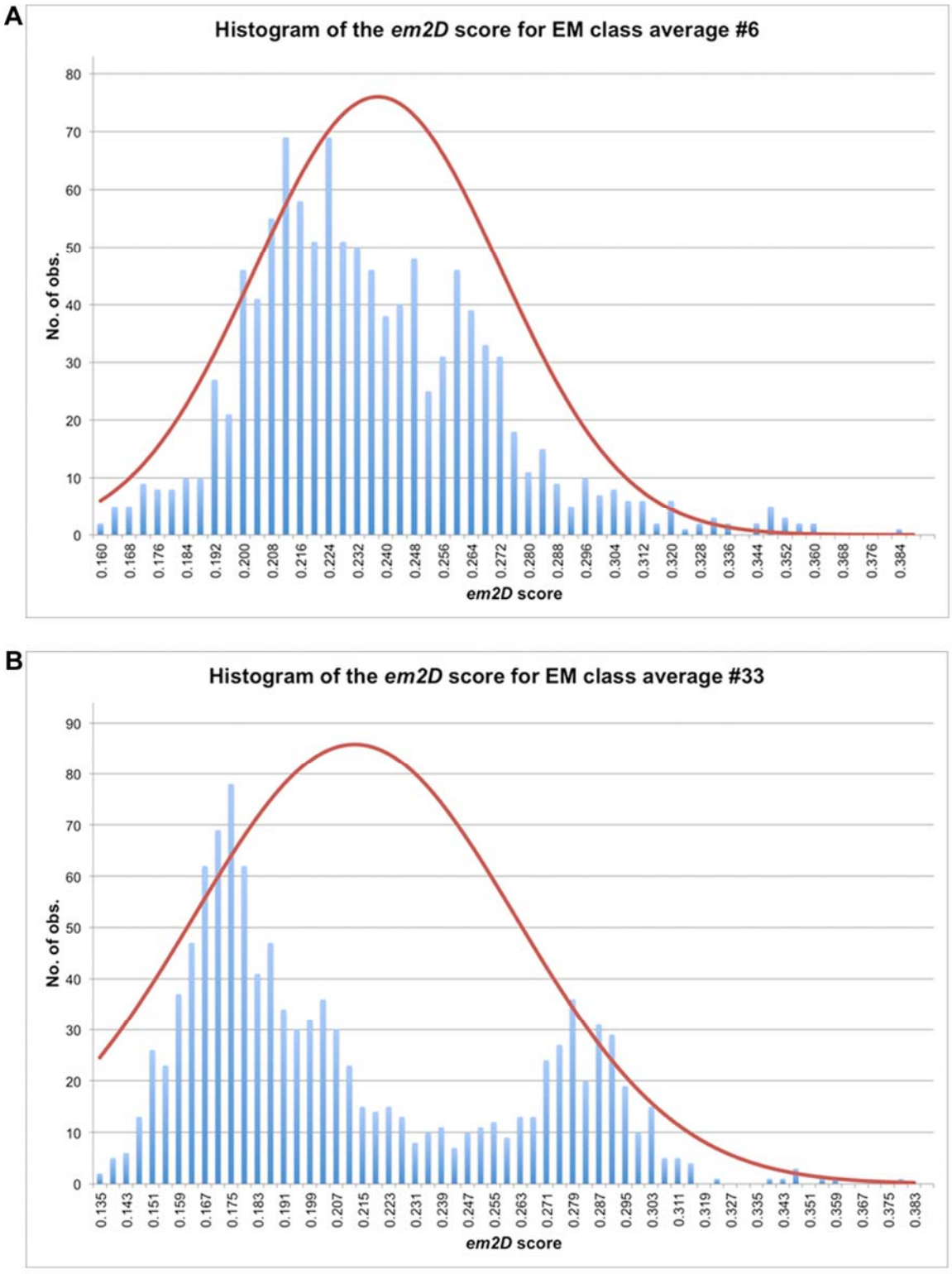

Supplementary Figure S5, Sampathkumar et al.,

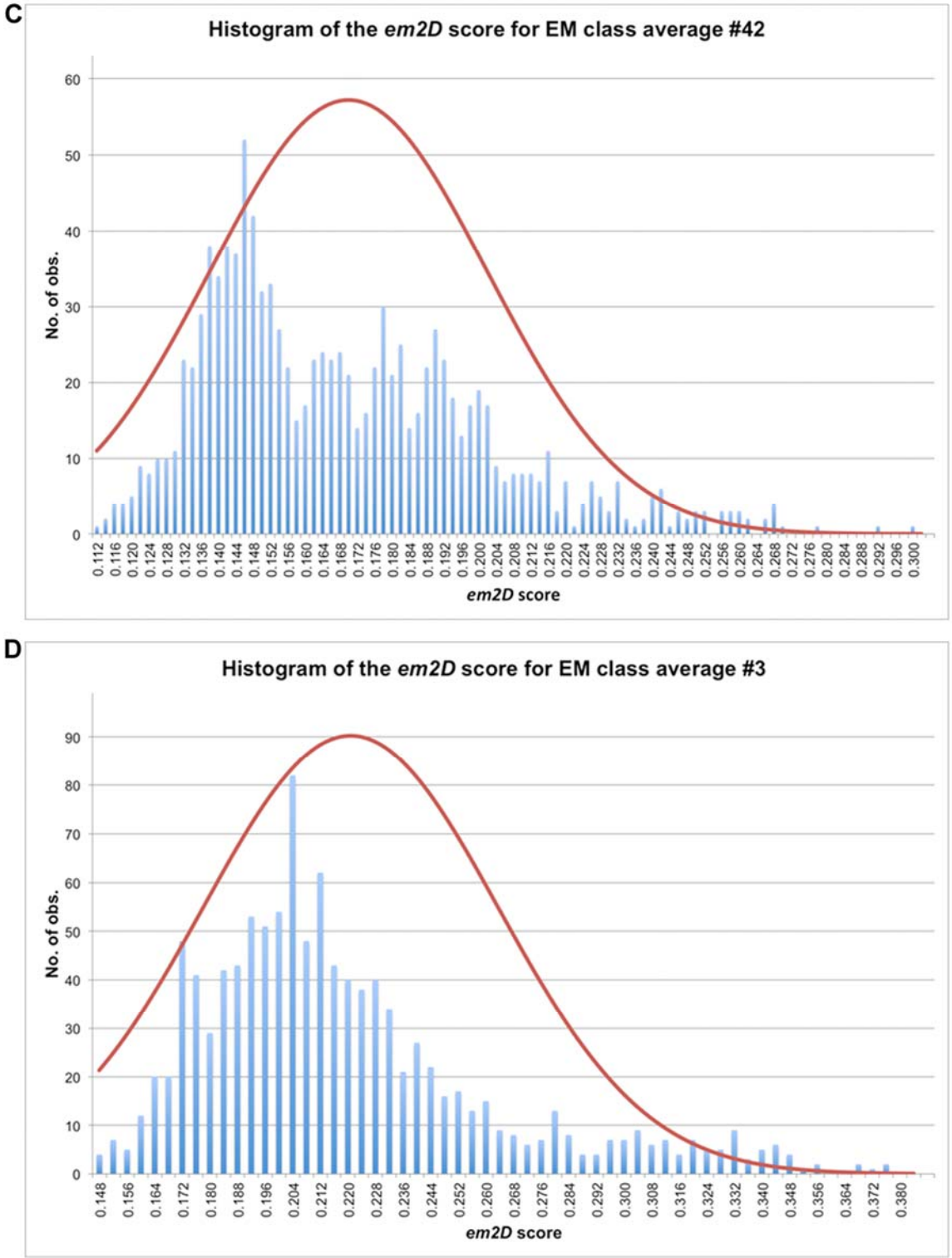

Supplementary Figure S5, Sampathkumar et al.,

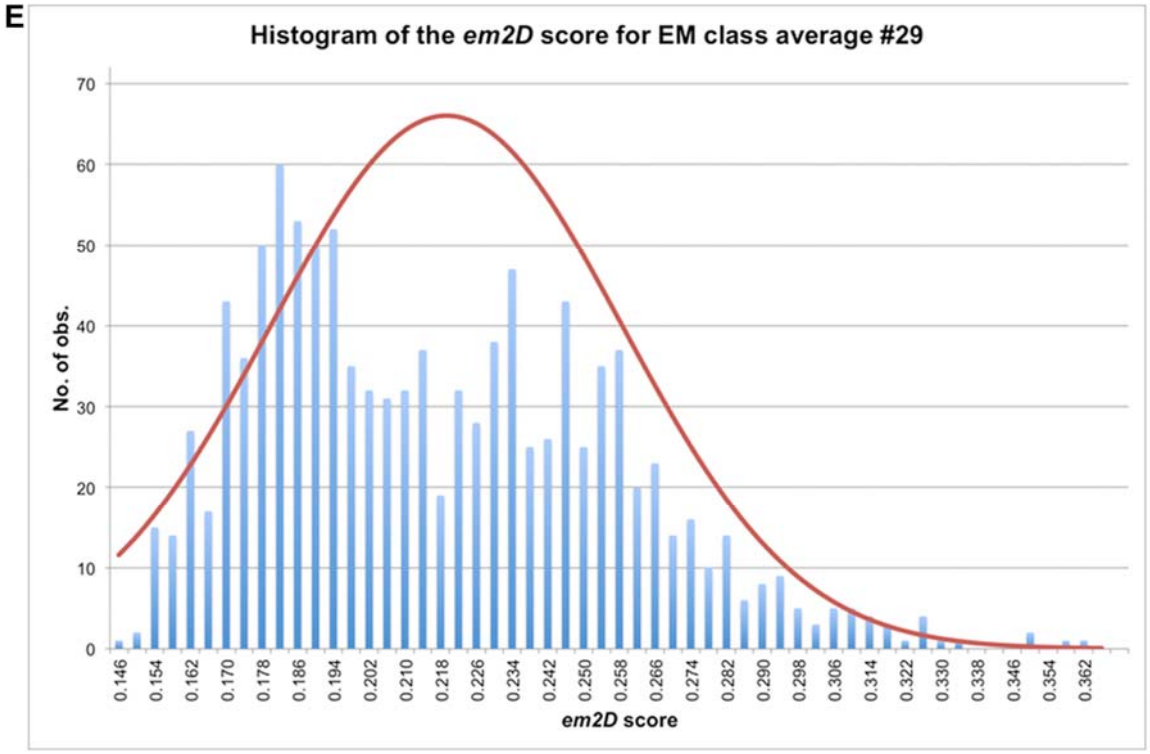

Figure S5, related to Figure 2. Histogram of *em2D* scores for selected class averages of ScNup192(2-960).

(A-E) The histograms (in blue bar) of the *em2D* scores (= 1 – the cross-correlation coefficient) for the EM class averages shown in Fig. 2b in the main text. The distributions of the *em2D* scores were determined from the pool of the crystal structure, the "complete model", and the 110,000 conformations (generated by the conformational sampling analysis using Molecular Dynamics). The overlapped red curve represents the Gaussian distribution function, calculated from the statistics of the *em2D* scores for each EM class average. The EM class averages 6 and 33 correspond to the "open" conformation (*em2D* scores of 0.202 and 0.137, respectively); EM class average 42 corresponds to the "closed" conformation (*em2D* score of 0.135), and EM class averages 3 and 29 correspond to the "complete" model (*em2D* scores of 0.161 and 0.179, respectively).

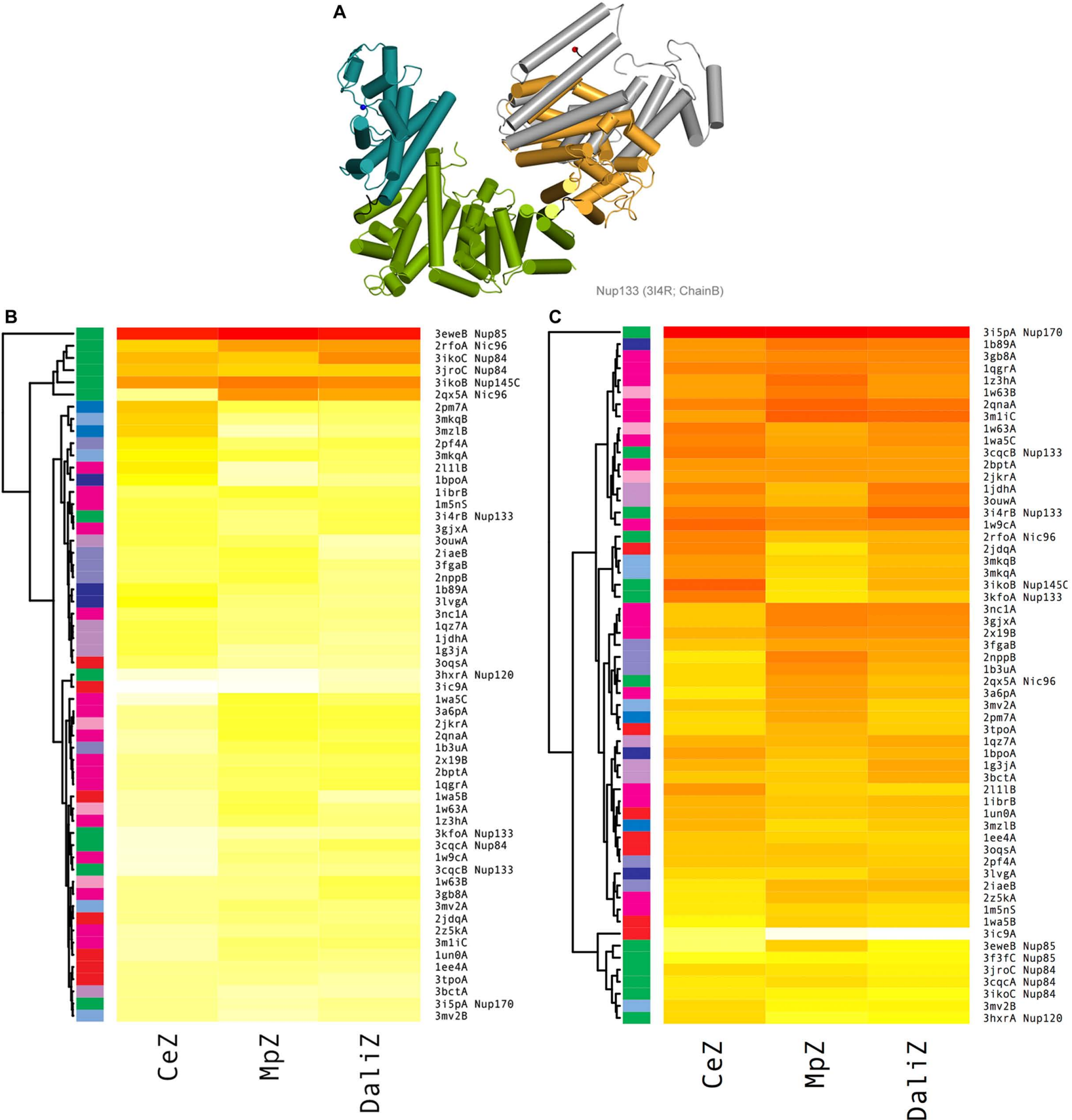
A
Nup133 (3I4R; ChainB)
B
3eweB Nup85
2rfoA Nic96
3ikoC Nup84
3jroC Nup84
3ikoB Nup145C
2qx5A Nic96
2pm7A
3mkqB
3mzlB
2pf4A
3mkqA
2l1lB
1bpoA
1ibrB
1m5nS
3i4rB Nup133
3gjxA
3ouwA
2iaeB
3fgaB
2nppB
1b89A
3lvgA
3nc1A
1qz7A
1jdhA
1g3jA
3oqsA
3hxrA Nup120
3ic9A
1wa5C
3a6pA
2jkrA
2qnaA
1b3uA
2x19B
2bptA
1qgrA
1wa5B
1w63A
1z3hA
3kfoA Nup133
3cqcA Nup84
1w9cA
3cqcB Nup133
1w63B
3gb8A
3mv2A
2jdqA
2z5kA
3m1iC
1un0A
1ee4A
3tpoA
3bctA
3i5pA Nup170
3mv2B
CeZ
MpZ
DaliZ
C
3i5pA Nup170
1b89A
3gb8A
1qgrA
1z3hA
1w63B
2qnaA
3m1iC
1w63A
1wa5C
3cqcB Nup133
2bptA
2jkrA
1jdhA
3ouwA
3i4rB Nup133
1w9cA
2rfoA Nic96
2jdqA
3mkqB
3mkqA
3ikoB Nup145C
3kfoA Nup133
3nc1A
3gjxA
2x19B
3fgaB
2nppB
1b3uA
2qx5A Nic96
3a6pA
3mv2A
2pm7A
3tpoA
1qz7A
1bpoA
1g3jA
3bctA
2l1lB
1ibrB
1un0A
3mzlB
1ee4A
3oqsA
2pf4A
3lvgA
2iaeB
2z5kA
1m5nS
1wa5B
3ic9A
3eweB Nup85
3f3fC Nup85
3jroC Nup84
3cqcA Nup84
3ikoC Nup84
3mv2B
3hxrA Nup120
CeZ
MpZ
DaliZ

Figure S6 related to Figure 3. Structural alignment of ScNup192(2-960) with Nup133 and heatmaps of structural comparisons with Nup85 and Nup170.

(A) Structural superposition for DALI alignment of Nup192(2-960) with Nup133 (PDB: 3I4R, chain B). The D1, D2, and D3 domains of ScNup192(2-960) structure shown in cyan, green, and gold, respectively, and Nup133 in grey.

(B-C) Heat map for structural comparisons to Nup85 and Nup170, respectively. Standardized scores for Dali, CE, and Multiprot alignments, along with the composite Z-score are represented as a yellow to red gradient; red indicates stronger alignment scores (**Table S4 and S5** for Nup85 and Nup170, repsectively). The structure dendrogram is computed by hierarchical clustering using pairwise distances between alignment Z-scores.

Supplementary Figure S7, Sampathkumar et al.,

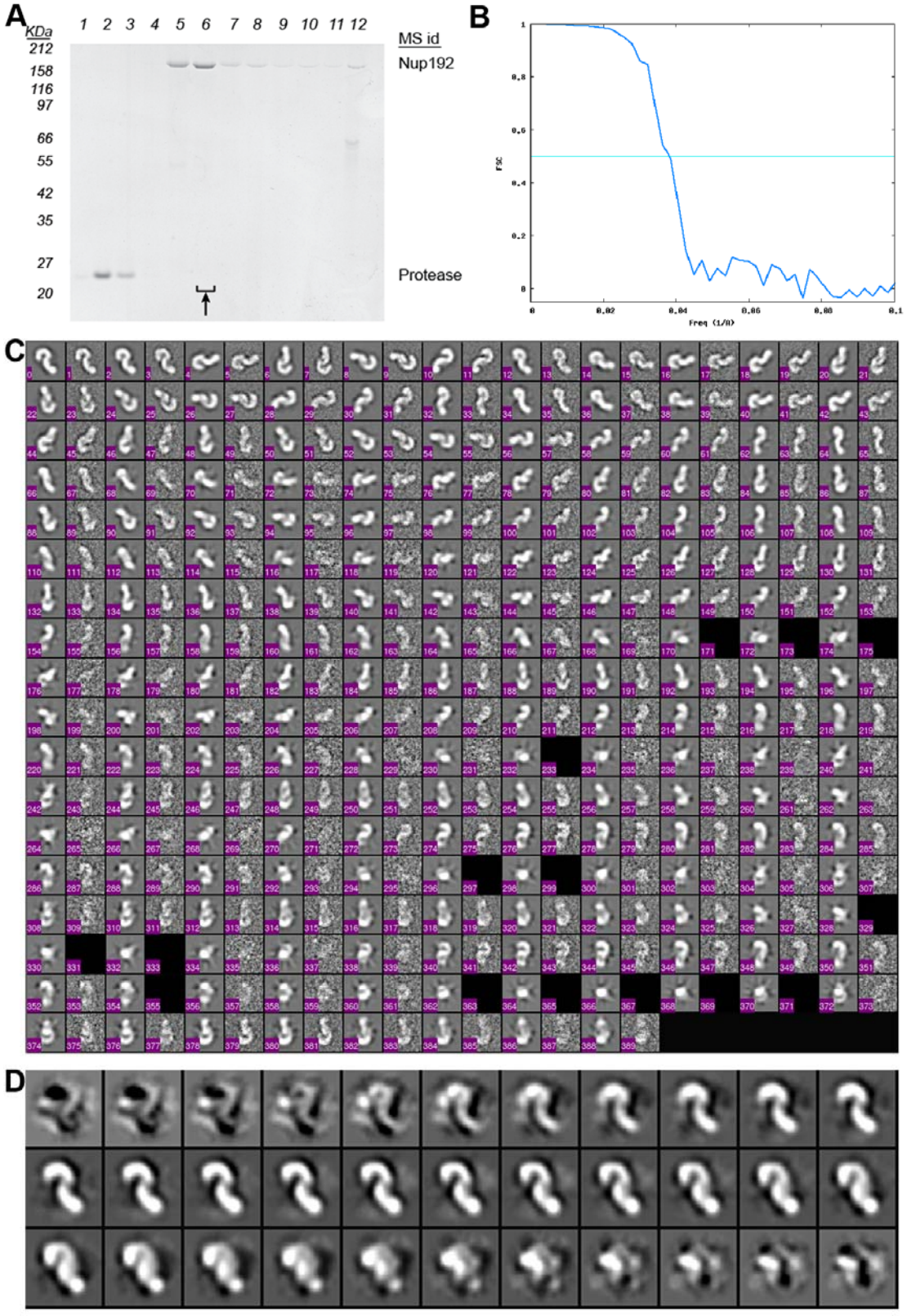

Figure S7 related to Figure 4. Structural model for the full length ScNup192 (ScNup192FL).

(A) SDS-PAGE image of ScNup192FL preparation stained with commassiae blue.

(B) Fourier shell correlation (FSC) plot for ScNup192FL. The FSC for the reconstruction was calculated by dividing the data set into equal halves and is plotted versus resolution (1/Å) in blue. The resolution at which it falls below 0.5 (cyan line) is taken to be the resolution of the reconstruction, 26Å in this case.

(C) Image showing projections of the final 3D reconstruction versus class averages for each projection. The first image of each pair is the projection (even numbers) and the second is the associated class average (odd numbers). At 10 degree angular intervals there were 195 projections. Black images show where no data matched a projection. The angular coverage was nearly complete and the class averages matched the projections well.

(D) Slices of ScNup192FL made through its 3D volume in the Z-direction.

Supplementary Figure S8, Sampathkumar et al.,

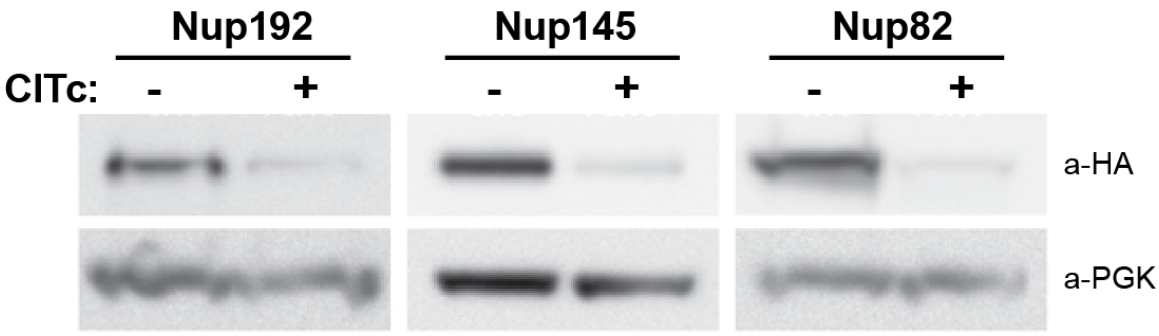

Figure S8 related to Figure 5. Analysis of the Nup protein levels after chlortetracycline treatment.

Western blot analysis showing the levels of HA-Nup192, HA-Nup145, and HA-Nup82 before (-) and after (+) treatment with chlortetracycline (ClTc). The upper row shows the signal for anti-HA antibody and the lower row a loading control showing the signal from an anti-Pgk1 antibody.

Caption for Supplementary Movies:

Supplementary Movie S1, S2, S3, S4, related to Figure 2: The supplementary movies 1-4 illustrate how 110,000 conformations were generated by molecular dynamics simulation. All the movies start from an initial model (the "complete" model, generated by MODELLER), which was subjected to energy minimization and heated up to 1,500K in the CHARMM force field (version 33b). The D1 and D3 domains were allowed to move relative to the D2 domain about the inter-domain loop residues 204-211 and 663-670, subject to an *Rg* constraint of 30 Å to 50 Å. Disordered loops not present in the crystal structure were also allowed to move. In the movies, we enforced the *Rg* constraints of 32 Å (movie 1), 36 Å (move 2), 40 Å (movie 3), and 50 Å (movie 4) to show the effect of the *Rg* constraints to the conformational sampling. All the movies were recorded by using VMD (Humphrey et al., 1996).

Supplementary Table S1: Data-collection and scattering-derived parameters for the SAXS experiment on ScNup192(2-960).

Data-collection parameters	
Instrument	SSRL BL4-2
Defining slit size (mm)	0.3(H) x 0.3(V)
Wavelength (Å)	1.12709
q range (Å^{-1})	0.0133 – 0.3098
Exposure time (sec)	1
Measurement repeats	24
Concentration range (mg ml^{-1})	0.4 – 2.5
Temperature (K)	288
Structural parameters †	
$I(0)$ (cm^{-1}) [from $P(r)$]	921.0 ± 2.872
R_g (Å) [from $P(r)$]	39.22 ± 0.090
$I(0)$ (cm^{-1}) (from Guinier)	921.1 ± 6.850
R_g (Å) (from Guinier)	39.30 ± 0.450
D_{max} (Å) ‡	123.0
Porod volume estimate (Å^3)	198530
Dry volume calculated from sequence (Å^3)	134377
Molecular-mass determination †	
Partial specific volume (cm^3 g^{-1})[1]	0.7586
Contrast ($\Delta\rho \times 10^{10}$ cm^{-2})	2.67
Molecular mass M_r [from $I(0)$]	107.51 kDa
Calculated monomeric M_r from sequence	111.06 kDa
Software employed	
Primary data reduction	*SASTOOL*
Data processing	*SASTOOL* and *PRIMUS*
Ab initio analysis (initial)	*DAMMIF*
Ab initio analysis (refinement)	*DAMMIN*
Validation and averaging	*DAMAVER*
Rigid-body modeling	N/A
Computation of model intensities	*FoXS*
3D graphics representations	*UCSF Chimera*

† Reported for the merged SAXS profile normalized at the concentration of 0.4 mg ml^{-1}.
‡ D_{max} is a model parameter in the $P(r)$ calculation and not all programs calculate an uncertainty associated with D_{max}. As such, it is reasonable to not cite an explicit error in D_{max}, although it may be useful to provide some estimate based on the results of $P(r)$ calculations using a range of D_{max} values.

Supplementary Table S2: The *em2D* scores (white background) with the rank percentage of a model (gray background) for each EM class average. The *em2D* score is defined as "one minus the cross-correlation coefficient between the image and the optimal model projection (1-ccc)", measuring the minimal difference between the image and a model projection. Table S2 summarizes the *em2D* scores for the "complete model", "open", and "closed" conformations for each EM class average, along with the rank (in percentage) of a model that is its position in the sorted list values of the *em2D* score. A number of EM class averages (highlighted in bold, with red color) were assigned to either the "complete" model, "open", or "closed" conformations. In general, a model of rank percentage of lower than ~20% can be presumably considered for the assignment of an EM class average.

Class ID	"complete" model		"open" conformation		"closed" conformation	
1	0.232	31.9%	**0.224**	**21.8%**	0.252	52.8%
2	0.167	4.0%	0.187	26.3%	0.159	0.8%
3	**0.161**	**1.4%**	0.200	34.0%	0.172	6.1%
4	0.236	33.3%	0.238	35.7%	0.211	12.9%
5	0.201	6.8%	0.219	18.9%	0.267	57.6%
6	0.232	48.8%	**0.202**	**12.3%**	0.231	47.8%
7	0.216	9.9%	0.302	92.1%	0.230	22.1%
8	0.280	91.7%	0.229	54.7%	0.219	43.6%
9	0.204	33.7%	0.169	0.6%	0.188	10.4%
10	0.140	15.4%	0.150	31.4%	0.148	26.0%
11	**0.193**	**3.4%**	0.250	40.7%	0.221	19.7%
12	0.244	50.5%	0.222	23.6%	0.208	12.0%
13	0.201	64.6%	**0.153**	**11.5%**	0.215	75.1%
14	0.218	19.1%	0.239	49.4%	0.274	86.8%
15	0.264	53.4%	0.242	24.9%	0.263	52.2%
16	0.173	16.6%	0.179	26.3%	0.195	54.8%
17	0.229	39.6%	0.232	42.9%	0.222	33.1%
18	0.172	5.5%	0.183	10.5%	0.196	18.4%

19	0.266	35.1%	0.307	65.1%	0.280	43.3%
20	0.242	41.2%	0.235	34.7%	0.281	65.3%
21	0.230	50.2%	**0.168**	**2.2%**	0.230	50.1%
22	0.259	44.2%	0.233	22.8%	0.231	21.7%
23	0.196	21.2%	0.217	64.1%	0.199	24.0%
24	0.222	31.4%	0.238	49.4%	0.249	61.3%
25	**0.178**	**18.7%**	0.194	50.1%	0.186	34.4%
26	0.198	18.3%	0.183	8.5%	0.274	89.5%
27	0.235	32.2%	0.217	18.2%	0.215	15.3%
28	0.315	84.5%	0.243	6.0%	0.283	49.7%
29	**0.179**	**14.5%**	0.184	20.9%	0.204	42.8%
30	0.145	8.1%	0.178	72.4%	0.159	29.8%
31	0.169	40.9%	0.165	37.4%	0.158	30.6%
32	0.152	28.4%	0.157	44.3%	0.156	40.8%
33	0.181	36.1%	**0.137**	**0.0%**	0.237	70.2%
34	0.257	47.1%	0.294	83.4%	0.250	37.4%
35	0.232	8.2%	0.258	36.2%	0.303	76.6%
36	0.261	25.0%	0.292	55.6%	0.292	55.5%
37	0.229	33.3%	0.237	41.6%	0.230	34.7%
38	0.236	24.7%	0.239	28.2%	0.261	50.2%
39	0.215	31.3%	**0.188**	**6.1%**	0.253	68.3%
40	0.239	44.8%	0.257	61.0%	0.323	82.6%
41	0.205	51.7%	0.248	88.6%	0.187	24.1%
42	0.157	43.8%	0.153	39.4%	**0.135**	**8.5%**
43	0.257	47.4%	0.199	3.8%	0.274	54.6%
44	0.207	11.8%	0.231	28.4%	0.205	9.7%
Average	0.214	31.9%	0.215	34.7%	0.226	41.0%

Supplementary Table S3. Structural similarity between ScNup192 and similar alpha-helical proteins.

PDB	DALI score	CE score	MultiProt score	Composite Z-score	Name	Class
1ee4A	13.2	6	213	1.4	SRP1_KAP60	kap
3oqsA	11.8	6.1	206	1.3	Impalpha2	kap
3tpoA	11.9	6	206	1.3	Impalpha2	kap
1un0A	11.8	5.9	209	1.3	SRP1_KAP60	kap
1wa5B	13.2	5.7	201	1.3	SRP1_KAP60	kap
1qz7A	13.9	5.7	177	1.2	Betacatenin	betacatenin
2jdqA	11.7	5.9	186	1.1	Impalpha1	kap
1jdhA	13.8	5.6	173	1.1	Betacatenin	betacatenin
3ouwA	11.9	5.7	183	1.0	Betacatenin	betacatenin
3nc1A	11.9	5.2	205	1.0	CRM1_KAP124	kap
1g3jA	13.8	5.3	172	1.0	Betacatenin	betacatenin
3bctA	13.3	5.5	167	1.0	Betacatenin	betacatenin
2bptA	11.8	4.9	217	1.0	KAP95	kap
2qnaA	13.3	5.2	173	0.9	KAP95	kap
1w63A	10	5.5	197	0.9	AP1	ap
1z3hA	10.5	5	211	0.9	CSE1_KAP109	kap
1w9cA	12.1	5.7	134	0.7	CRM1_KAP124	kap
1wa5C	13	3.9	218	0.7	CSE1_KAP109	kap
3m1iC	9.8	5	198	0.7	CRM1_KAP124	kap
2z5kA	12	4.4	199	0.7	Transportin1	kap
1m5nS	10.2	5.2	177	0.7	KAP95	kap
1ibrB	11.1	5.2	165	0.7	KAP95	kap
1qgrA	11.4	4.4	202	0.7	KAP95	kap
3gjxA	10	4.6	202	0.6	CRM1_KAP124	kap
3gb8A	11.3	3.9	198	0.4	CRM1_KAP124	kap
2jkrA	9.2	5.2	153	0.4	AP2	ap
3a6pA	8.8	5	158	0.4	Expotin5	kap
2x19B	9.6	4.7	160	0.3	Imp13	kap
1b3uA	7	5	151	0.2	PP2A	pp2
2iaeB	7.9	5	139	0.2	PP2A	pp2
2pf4A	6.3	4.7	171	0.1	PP2A	pp2
1w63B	8	4.6	152	0.1	AP1	ap
3fgaB	8	4.4	143	0.0	PP2A	pp2
2nppB	7.5	4.4	143	-0.1	PP2A	pp2
3cqcA	3.2	5.2	73	-0.6	Nup84	nup
3mv2B	3	4.6	94	-0.7	COP1	copI
3i4rB	5.2	3.9	100	-0.7	Nup133	nup
1b89A	3.5	3.9	87	-0.9	CHC1	clathrin
2rfoA	4.9	3.3	95	-1.0	Nic96	nup
3hxrA	2.4	4.1	84	-1.0	Nup120	nup

3i5pA	3.7	3.7	87	-1.0	Nup170	nup
3lvgA	4.4	3.5	88	-1.0	CHC1	clathrin
3kfoA	2.5	4.3	65	-1.0	Nup133	nup
1bpoA	2.9	3.7	83	-1.1	CHC1	clathrin
3ikoB	1.7	4.1	76	-1.1	Nup145C	nup
3mzlB	1.2	4.3	71	-1.3	SEC31	copII
2pm7A	3.3	3.9	64	-1.3	SEC31	copII
3cqcB	4	3.7	61	-1.5	Nup133	nup
3ikoC	2.5	3.5	72	-1.5	Nup84	nup
2qx5A	4.8	2.6	88	-1.5	Nic96	nup
3mv2A	2.9	3.3	68	-1.6	COP1	copI
3mkqA	2.2	2.8	82	-1.8	COP1	copI
3jroC	4.2	2.6	66	-1.3	Nup84	nup
3mkqB	1.9	3.1	64	-1.3	COP1	copI
3f3fC	2.2	2.6	70	-1.5	Nup85	nup
3eweB	3.2	2	69	-1.5	Nup85	nup

Supplementary Table S4. Structural similarity between ScNup85 and similar alpha-helical proteins.

PDB	DALI Score	CE Score	MultiProt Score	Composite Z-score	Name	Class
3ikoB	14.3	5.9	141	1.44	Nup145C	nup
3ikoC	14.2	5.2	105	1.02	Nup84	nup
2rfoA	13	4.7	124	0.93	Nic96	nup
3jroC	9.6	5	101	0.75	Nup84	nup
2qx5A	12.4	2.8	129	0.36	Nic96	nup
2pm7A	4.5	4.9	72	0.34	SEC31	copII
3mkqB	4.2	4.7	63	0.22	COP1	copI
3mzlB	3.7	4.7	56	0.16	SEC31	copII
2pf4A	4.9	4.1	67	0.09	PP2A	pp2
3mkqA	4.4	3.9	74	0.05	COP1	copI
2l1lB	4.3	4.1	55	0.00	CRM1_KAP124	kap
3lvgA	3.4	3.7	65	-0.10	CHC1	clathrin
1b89A	3.6	3.5	68	-0.13	CHC1	clathrin
1m5nS	4.8	3.3	69	-0.14	KAP95	kap
1bpoA	3.4	3.7	56	-0.15	CHC1	clathrin
3i4rB	4.9	3.3	64	-0.16	Nup133	nup
3gjxA	4.8	3.3	64	-0.17	CRM1_KAP124	kap
1ibrB	4.5	3.1	75	-0.18	KAP95	kap
1qz7A	3.5	3.3	65	-0.21	Betacatenin	betacatenin
3fgaB	3.8	3.1	72	-0.22	PP2A	pp2
3ouwA	2.6	3.3	69	-0.23	Betacatenin	betacatenin
2nppB	3.5	3.1	73	-0.23	PP2A	pp2
1jdhA	3.1	3.3	65	-0.23	Betacatenin	betacatenin
2jkrA	5.2	2.8	75	-0.24	AP2	ap
3a6pA	5.2	2.8	75	-0.24	Expotin5	kap
2iaeB	2.9	3.1	74	-0.25	PP2A	pp2
1g3jA	3.3	3.3	59	-0.26	Betacatenin	betacatenin
3nc1A	3.7	3.1	64	-0.27	CRM1_KAP124	kap
2bptA	4.8	2.8	69	-0.29	KAP95	kap
1qgrA	4.9	2.8	68	-0.29	KAP95	kap
2x19B	4.5	2.8	67	-0.31	Imp13	kap
2qnaA	4.7	2.6	75	-0.32	KAP95	kap
1w63B	4.9	2.8	63	-0.32	AP1	ap
3oqsA	3.1	3.1	60	-0.32	Impalpha2	kap
1b3uA	5.1	2.6	70	-0.33	PP2A	pp2
3gb8A	4.7	2.8	62	-0.33	CRM1_KAP124	kap
3mv2A	3.8	2.8	67	-0.34	COP1	copI
2jdqA	3.7	2.8	65	-0.36	Impalpha1	kap
1w63A	3.7	2.6	72	-0.38	AP1	ap
1ee4A	3.4	2.8	63	-0.38	SRP1_KAP60	kap
3m1iC	4.3	2.6	67	-0.38	CRM1_KAP124	kap

1z3hA	3.9	2.6	69	-0.38	CSE1_KAP109	kap
3i5pA	3.5	2.8	58	-0.40	Nup170	nup
3tpoA	2.9	2.8	62	-0.41	Impalpha2	kap
1un0A	3.7	2.6	66	-0.41	SRP1_KAP60	kap
1wa5C	4.4	2.3	75	-0.42	CSE1_KAP109	kap
2z5kA	4	2.6	62	-0.42	Transportin1	kap
1wa5B	2.7	2.6	71	-0.42	SRP1_KAP60	kap
3mv2B	3.3	2.8	56	-0.42	COP1	copI
3bctA	2.8	2.8	57	-0.44	Betacatenin	betacatenin
3cqcA	4.6	2.3	63	-0.48	Nup84	nup
1w9cA	3.9	2.3	65	-0.50	CRM1_KAP124	kap
3cqcB	3.5	2.3	62	-0.53	Nup133	nup
3kfoA	3.1	2.3	58	-0.57	Nup133	nup
3hxrA	2.4	2.3	48	-0.66	Nup120	nup
3ic9A	2.6	2	47	-0.74	ExportinT	kap

Supplementary Table S5. Structural similarity between ScNup170 and similar alpha-helical proteins.

PDB	DALI Score	CE Score	MultiProt score	Composite Z-score	Name	Class
3i4rB	4.9	4.7	102	0.41	Nup133	nup
1w9cA	5	4.9	75	0.32	CRM1_KAP124	kap
1jdhA	3.9	4.6	102	0.30	Betacatenin	betacatenin
2qnaA	5.9	4.6	83	0.28	KAP95	kap
3m1iC	6	4.3	96	0.24	CRM1_KAP124	kap
1w63A	4.3	4.7	82	0.23	AP1	ap
3ikoB	3	5	71	0.22	Nup145C	nup
3ouwA	4	4.4	101	0.21	Betacatenin	betacatenin
1qgrA	5.3	4.6	76	0.20	KAP95	kap
1wa5C	4.4	4.6	83	0.20	CSE1_KAP109	kap
1b89A	5.5	4.4	86	0.19	CHC1	clathrin
3cqcB	4.6	4.7	70	0.16	Nup133	nup
3gb8A	5.1	4.4	86	0.16	CRM1_KAP124	kap
2jdqA	3	4.6	82	0.11	Impalpha1	kap
2bptA	4.7	4.4	78	0.09	KAP95	kap
2rfoA	3.8	4.6	71	0.08	Nic96	nup
1w63B	5.4	4.3	75	0.06	AP1	ap
1z3hA	5.7	4.3	71	0.05	CSE1_KAP109	kap
2jkrA	4.6	4.3	79	0.04	AP2	ap
2x19B	4.9	4.1	89	0.03	Imp13	kap
3mkqA	3.2	4.4	80	0.01	COP1	copI
3nc1A	5.2	3.9	97	0.01	CRM1_KAP124	kap
3kfoA	2.9	4.7	62	0.01	Nup133	nup
3gjxA	5.2	3.9	94	-0.01	CRM1_KAP124	kap
1g3jA	3.5	4.1	94	-0.01	Betacatenin	betacatenin
1bpoA	3.8	4.3	77	-0.02	CHC1	clathrin
3mkqB	3.4	4.4	73	-0.02	COP1	copI
1qz7A	4	4.1	86	-0.04	Betacatenin	betacatenin
3fgaB	4.5	3.9	88	-0.09	PP2A	pp2
3bctA	3.6	3.9	94	-0.10	Betacatenin	betacatenin
1ibrB	3.7	4.1	78	-0.11	KAP95	kap
1un0A	3.6	4.1	75	-0.14	SRP1_KAP60	kap
2l1lB	3.5	4.4	54	-0.15	CRM1_KAP124	kap
3mzlB	3.2	4.1	76	-0.16	SEC31	copII
1b3uA	4.9	3.7	80	-0.22	PP2A	pp2
2nppB	5.2	3.5	88	-0.24	PP2A	pp2
2pf4A	3.7	3.9	73	-0.24	PP2A	pp2
3oqsA	3.8	3.9	70	-0.26	Impalpha2	kap
3lvgA	3.2	3.7	88	-0.26	CHC1	clathrin
2qx5A	4.6	3.7	75	-0.27	Nic96	nup
1ee4A	3.4	3.9	71	-0.27	SRP1_KAP60	kap

2iaeB	4	3.5	92	-0.28	PP2A	pp2
3mv2A	4.4	3.9	61	-0.29	COP1	copI
3a6pA	4.6	3.5	83	-0.31	Expotin5	kap
3tpoA	4.1	3.7	72	-0.32	Impalpha2	kap
2pm7A	4.4	3.7	68	-0.33	SEC31	copII
2z5kA	3.9	3.5	80	-0.37	Transportin1	kap
1m5nS	3.4	3.5	75	-0.43	KAP95	kap
3mv2B	2.4	3.7	63	-0.48	COP1	copI
3jroC	3	3.7	58	-0.48	Nup84	nup
1wa5B	3.5	3.3	78	-0.50	SRP1_KAP60	kap
3hxrA	1.9	3.7	61	-0.52	Nup120	nup
3cqcA	3.2	3.5	63	-0.53	Nup84	nup
3ikoC	2.5	3.5	56	-0.62	Nup84	nup
3f3fC	2.4	3.1	74	-0.69	Nup85	nup
3eweB	3.5	2.8	67	-0.81	Nup85	nup
3ic9A	0.4	2.8	45	-1.15	ExportinT	kap

Table S6. Nup192 Segment Models

Template PDB	Nup192 Segment	Alignment %id
1wa5C	981-1070	11.7
1u6gC	1075-1345	11.2
3grlA	1371-1674	9.3

Supplementary Experimental Procedures

Cloning, Expression, Purification, and Crystallization of ScNup192(2-960)

The gene encoding Nup192 from *S. cerevisiae* was cloned from genomic DNA of strain 2601D-5 (ATCC, USA). The domain encoding residues 2-960 [ScNup192(2-960)] was PCR amplified using AAATGGTCTGCAATTCCTTTCC and CAGACAAAGACGCAACGGAGCCA as forward and reverse primers, respectively. The purified PCR product was TOPO® (Invitrogen, USA) cloned into pSGX3, a derivative of pET26b(+), yielding a protein with a non-cleavable C-terminal hexa-histidine tag. The resulting plasmid was transformed into BL21(DE3)-Condon+RIL (Invitrogen, USA) cells for expression. Production of Se-Met protein (Van Duyne et al., 1993) was carried out in 1L of HY media at 22ºC containing 50µg/mL of kanamycin and 35µg/mL of chloramphenicol. Protein expression was induced by addition of 0.4mM IPTG. Cells were harvested after 21 hours by centrifugation at 4ºC.

For purification, 18g of *E. coli* cell pellet was resuspended in 200mL of cold buffer containing 20mM Tris HCl *p*H 8.0, 500mM NaCl, 25mM imidazole, 2mM $MgCl_2$, 0.5mM ATP, 0.5mM TCEP, and 0.1% (v/v) Tween20, and incubated with DNAaseI (Roche, USA) for 30 minutes in the presence of EDTA-free complete protease inhibitor cocktail tablets (Roche, USA) at 4ºC. Cells were ruptured using an Avestin EmulsiFlex-C3 homogenizer and debris was removed by centrifugation at 4ºC. The supernatant was batch bound to 7mL of Ni-NTA resin (Qiagen, USA) pre-equilibrated with 25mM imidazole in Buffer1 (20mM Tris HCl *p*H 8.0, 500mM NaCl, 10% (v/v) glycerol, 0.5mM TCEP). The sample was washed with 100 mL of 50mM imidazole in Buffer1, and subsequently eluted with 30 mL of 250mM imidazole in the Buffer1. Eluted protein was

further purified over a 120 mL Superdex 200 column equilibrated with 20 mM HEPES *p*H 8.0, 500 mM NaCl, 10% (v/v) glycerol, and 5mM DTT containing four complete protease inhibitor tablets in 400 mL (protein storage buffer). Elution fractions, analyzed by SDS-PAGE, were combined and concentrated and aliquots were frozen in liquid nitrogen for storage at -80ºC.

Crystallization and Structure Determination of ScNup192(2-960)

Screening of ScNup192(2-960), (at 8.84 mg/mL), was carried out using MCSG1-4 crystallization formulations (Microlytic, USA), dispensed with a Phoenix Liquid Handling System (Art Robins, USA) *via* sitting drop vapor diffusion at 21ºC (0.3 µL protein + 0.3 µL reservoir solution). Screen conditions which gave initial crystals were extensively optimized to improve diffraction. Diamond-like crystals were obtained from sitting drops with 10% to 20% PEG3350 in presence of variety of mono-valent ions (typically 1µL of reservoir solution combined with 1µL of protein). The sample (crystal number 1) used for Se-SAD structure solution appeared in the presence of 14 % PEG3350 and 200 mM potassium sulfate, and diffracted to 3.4 Å resolution in the presence of ~20 % (v/v) glycerol as cryoprotectant. The sample used for final refinment at 3.25 Å resolution (crystal number 2) grew in the presence of 10% PEG3350 and 100mM potassium iodide. This crystal was equilibrated against a solution of saturated ammonium sulfate for 2.5 hours, before being flash frozen in liquid nitrogen with 30% PEG400 and 25% of saturated ammonium sulfate as cryo-protectant.

Diffraction data sets were recorded at both the X29A (Brookhaven National Laboratory) and the LRL-CAT 31-ID (Advanced Photon Source) beamlines and processed with HKL3000 (Minor et al., 2006). Diamond-like crystals belong to the

$P4_32_12$ space group with one molecule of ScNup192(2-960) in the asymmetric unit. A selenium sub-structure solution was obtained using the AutoSol wizard (Terwilliger et al., 2009; Zwart et al., 2008) in Phenix (Adams et al., 2010) with resolution limit set to 3.7 Å for the heavy atom search. Subsequent density modification resulted in an electron density map with clearly defined secondary structural elements and discernable sidechain density features (**Figure S1**). Initial model building was carried out using both the AutoBuild wizard (Afonine et al., 2012; Terwilliger et al., 2008) in Phenix, and Buccaneer (Cowtan, 2008) as implemented in CCP4 (Potterton et al., 2003; Winn et al., 2011). The resulting models were manually edited and combined to assemble a model of ScNup192(2-960) which was complete except for N-terminal 145 residues and disordered loops. This model was refined against the dataset from crystal number 2. Subsequent model completion involved map improvement by atom update in ARP/wARP (Langer et al., 2008; Morris et al., 2003) and solvent flattening in Parrot (Zhang et al., 1997), and manual building in COOT (Emsley and Cowtan, 2004; Emsley et al., 2010) followed by refinement using Refmac5 (Murshudov et al., 1997). Illustrations were prepared using PyMol (DeLano, 2002) and Chimera (Pettersen et al., 2004).

Small Angle X-ray Scattering (SAXS)

SAXS measurements of ScNup192(2-960) were carried out at Beamline 4-2 of the Stanford Synchrotron Radiation Lightsource (SSRL), SLAC National Accelerator Laboratory. The beam energy and current were 11 keV and 300mA, respectively. A silver behenate sample was used to calibrate the ***q***-range and detector distance. Data collection was controlled with Blu-Ice (McPhillips, et al., 2002). We used an automatic sample delivery system equipped with a 1.5 mm-diameter thin-wall quartz capillary within which

a sample aliquot was oscillated in the X-ray beam to minimize radiation damage. The sample was placed at 1.7 m from a Rayonix MX225-HE (MAR-USA, USA) CCD detector with a binned pixel size of 293 μm by 293 μm. For more details of other parameters, see Table S1.

All protein samples for the SAXS experiment were suspended in the protein storage buffer, composed of 20 mM HEPES at pH 8.0, 500 mM NaCl, 10 % (v/v) glycerol, and 5 mM DTT containing four complete protease inhibitor tablets in 400 mL. All the suspensions were filtered through 0.1 μm membranes (Millipore, Bedford, MA) and a total of 10% glycerol was added to reduce radiation damage (Kuwamoto et al., 2004). Each of the 24 scattering images was scaled by the transmitted beam intensity, using SASTool (http://ssrl.slac.stanford.edu/~saxs/analysis/sastool.htm, formerly MarParse), and averaged to obtain fully processed data in the form of intensity *versus* $\boldsymbol{q}$ [$\boldsymbol{q}=4\pi\sin(\theta)/\lambda$, where θ is one-half of the scattering angle and λ is the X-ray wavelength]. The average of the lower scattering angle parts ($\boldsymbol{q}<0.15\text{Å}^{-1}$) of the lower concentration profiles (0.4-1.0 mg/mL) and the average of the higher scattering angle parts ($\boldsymbol{q}>0.12\text{Å}^{-1}$) of the higher concentration (1.5-2.5 mg/mL) profiles were merged to obtain the final experimental SAXS profile.

The merged experimental SAXS profile was compared with SAXS profiles calculated using the crystal structure of ScNup192(2-960) with FoXS program (http://salilab.org/foxs). In addition, 1,000 monomer models of ScNup192(2-960) which included a C-terminal hexa-histidine tag (Gly-His-His-His-His-His-His), 113 disordered residues (not modeled in the crystal structure), missing side-chains, and 8 Se-Met residues, were generated using the crystal structure with the automodel function of

MODELLER and customized scripts in IMP, and compared with the merged experimental SAXS profile. A "complete model" was chosen as having the smallest chi value (χ = 3.84) among the 1,000 monomer models. The *ab initio* shape of ScNup192(2-960) was initially computed from the merged experimental SAXS profile by running DAMMIF (Franke, 2009) 20 times, and further refined with additional 50 DAMMIN (Svergun, 1999) runs, followed by superposition and averaging with DAMAVER (Volkov, 2003). Fittings of models into the *ab initio* shape were visualized by customized scripts in UCSF Chimera (Pettersen et al., 2004).

Negative Staining and EM analyses of ScNup192(2-960)

Purified recombinant ScNup192(2-960) was applied to glow-discharged carbon-coated copper grids. The grids were rinsed with four drops of 0.75-1% uranyl formate, then stained for a minute and air-dried. The images of ScNup192(2-960) were collected on a Tecnai F20 (FEI Inc., USA) transmission electron microscope operating at an accelerating voltage of 80 kV at 50,000x magnification and underfocus ~1 μm. Images were recorded on a Tietz F224 4096x4096 CCD camera (15 um pixels) at 2X binning. The pixel size at the specimen level was 3.23 Å. Particles were selected using Boxer from EMAN (Ludtke et al., 1999). The contrast transfer function (CTF) of the images was determined using ctfit from EMAN and the phases flipped accordingly. The particles were normalized and were then subjected to the Iterative Stable Alignment and Clustering (ISAC; (Yang et al., 2012) technique to produce stable class averages. The program was run for 7 generations in total; after each generation stable particles were

removed from the stack and the program was re-run with unclassified particles until no new classes were found. A pixel error of $2\sqrt{3}$ was used for the stability threshold.

We quantified the overlap of projections of the "complete model" and the 110,000 MD generated conformations of ScNup192(2-960) with each of 44 EM class averages, using the *EMageFit* application (Velazquez-Muriel et al., 2012) of the Integrative Modeling Platform (IMP) software package (Russel et al., 2012) (**Figure S4; Table S2**). First, an atomic model was downsampled to a resolution of 15 Å and projected in all directions of the hemisphere. Second, a coarse registration between each projection and a class-average was performed. Finally, the best coarse match was refined by the Simplex algorithm to obtain the *em2D score*. The *em2D* score is defined as one minus the cross-correlation coefficient between the image and the best-matching projection. The histograms of the *em2D* scores for all class averages were generated to determine the best matching conformation (or subset conformations), while selected histograms are shown (**Figure S5**). In general, a model can be considered for assignment to a class average if its rank percentage is lower than ~20%.

Purification and 3D EM Construction of Native, full-length *S. cerevisiae* Nup192 (ScNup192FL).

To purify native Nup192, we constructed a strain in which the NUP encoding gene was genomically tagged with PrA preceded by the human rhinovirus 3C protease (ppx) target sequence (GLEVLFQGPS) as described previously (Fernandez-Martinez et al., 2012). The ScNup192FL was isolated by affinity purification using IP buffer (20mM Hepes, 300mM NaCl, 2mM $MgCl_2$, 0.5% Triton, 0.1% Tween 20, 1mM DTT) and released from the affinity matrix by protease digestion in digestion buffer (20mM Hepes,

300mM NaCl, 2mM $MgCl_2$, 0.01% Tween 20, 0.1mM DTT). The recovered sample was then centrifuged at 20,000 g for 10 min. The supernatant was loaded on top of a 5-20% sucrose gradient made with digestion buffer plus 1/1000 protease inhibitors. Gradients were ultracentrifuged on a SW55 Ti rotor (Beckman-Coulter) at 50,000 rpm and 5°C for 10 hours. Gradients were manually unloaded from the top into 12 fractions of 410 μL. Fractions were analyzed by SDS-PAGE, R250 Coomassie staining and mass spectrometry.

Purified, native ScNup192FL was applied to glow-discharged carbon-coated copper grids. The grids were rinsed with four drops of 0.75-1% uranyl formate, then stained for a minute and air-dried. The random conical tilt reconstruction method was used to create an initial model of ScNup192FL (Frank and Radermacher, 1992). A JEOL JEM-2100F transmission electron microscope (JEOL USA Inc., Peabody MA) operating at an accelerating voltage of 200 kV was used to image ScNup192FL. The image pairs were recorded at 50° and 0° under low-dose conditions and 50,000x magnification using underfocus values between 1 and 2 μm. Images were recorded on a Tietz F224HD 2048x2048 CCD camera with 24 μm pixels (Tietz Video and Image Processing Systems GmbH, Germany). The pixel size at the specimen level was 2.93 Å. Tilt pairs were selected using JWEB and windowed using SPIDER (Frank et al., 1996). The images were shrunk by a factor of 2 followed by one generation of classification of untilted images using the ISAC method. Three class averages comprising 120, 100 and 42 particles were chosen for 3D reconstruction using associated tilted images and calculated Euler angles. The three reconstructions were aligned using Chimera (Pettersen et al., 2004) and averaged, and this combined reconstruction was used as an initial model for reference

based alignment in SPIDER (Frank et al., 1996). A total of 3883 particles were used in the refinement: 676 tilted, 676 untilted, and an additional 2351 untilted particles picked with Boxer. Slices of ScNup192FL were made through its 3D volume in the Z direction using SPIDER (Frank et al., 1996).

Functional analysis of ScNup192

The Nab2NLS-mCherry-PrA reporter protein is a tandem fusion of the NLS of Nab2, mCherry and a single repeat motif of PrA, constructed from a Nab2NLS-GFP-PrA expression plasmid (pBT016; Timney, et al., 2006), and subcloned into a centromeric yeast plasmid for expression from a constitutive TEF1 promotor (pBT054). Conditional mutants of Nup192, Nup145 and Nup82 were engineered by inserting 3 tetracycline-binding aptamers (3tc-apts) and 3xHA tag upstream of the corresponding open reading frames with homologous recombination tagging in DF5α strain. Recombination cassettes were PCR-amplified from pTDH3-tc3-3xHA (Euroscarf). Oligonucleotide sequences are available upon request. Tetracycline-repressible Nup192, Nup145 and Nup82 strains and WT cells, transformed with the NLS-mCherry reporter plasmid, were grown to log phase in synthetic complete media, diluted to 0.25 x 10^7 cells/mL, and treated with 0.2 mg/mL chlorotetracycline. Treated cultures were then incubated at 30ºC for 24 hours. Samples of cultures for imaging were transferred to Concanavalin A coated glass-bottomed culture dishes for imaging (Zenklusen, et al., 2007). Images were collected of >100 cells after 0 hours and 24 hours of treatment. Z-stacks of cell-fields were collected on a Zeiss Axioplan 200 inverted microscope fitted with a Perkin-Elmer UltraView spinning disk confocal imaging head using a 100x 1.45NA objective collected with a Andor iXon

EMCCD camera. Image stacks were background subtracted, adjusted for flat field illumination and combined into single images using maximum-intensity projection. Nuclear and cytoplasmic regions from all cells in these images were segmented using purpose-built MatLab scripts, and the mean pixel intensities from the segmented images used to calculate the N/C reporter-protein ratio for each cell.

Supplementary References

Adams, P.D., Afonine, P.V., Bunkoczi, G., Chen, V.B., Davis, I.W., Echols, N., Headd, J.J., Hung, L.W., Kapral, G.J., Grosse-Kunstleve, R.W., *et al.* (2010). PHENIX: a comprehensive Python-based system for macromolecular structure solution. Acta Crystallogr. D Biol. Crystallogr. *66*, 213-221.

Afonine, P.V., Grosse-Kunstleve, R.W., Echols, N., Headd, J.J., Moriarty, N.W., Mustyakimov, M., Terwilliger, T.C., Urzhumtsev, A., Zwart, P.H., and Adams, P.D. (2012). Towards automated crystallographic structure refinement with phenix.refine. Acta Crystallogr. D Biol. Crystallogr. *68*, 352-367.

Cowtan, K. (2008). Fitting molecular fragments into electron density. Acta Crystallogr. D Biol. Crystallogr. *64*, 83-89.

DeLano, W.L. The PyMOL Molecular Graphics System (2002) DeLano Scientific, San Carlos, CA, USA. http://www.pymol.org.

Emsley, P., and Cowtan, K. (2004). Coot: model-building tools for molecular graphics. Acta Crystallogr. D Biol. Crystallogr. *60*, 2126-2132.

Emsley, P., Lohkamp, B., Scott, W.G., and Cowtan, K. (2010). Features and development of Coot. Acta Crystallogr. D Biol. Crystallogr. *66*, 486-501.

Fernandez-Martinez, J., Phillips, J., Sekedat, M.D., Diaz-Avalos, R., Velazquez-Muriel, J., Franke, J.D., Williams, R., Stokes, D.L., Chait, B.T., Sali, A., *et al.* (2012). Structure-function mapping of a heptameric module in the nuclear pore complex. J. Cell Biol. *196*, 419-434.

Frank, J., & Radermacher, M. (1992). Three-dimensional reconstruction of single particles negatively stained or in vitreous ice. Ultramicroscopy, *46(1-4)*, 241-262.

Frank, J., Radermacher, M., Penczek, P., Zhu, J., Li, Y., Ladjadj, M., and Leith, A. (1996) SPIDER and WEB: processing and visualization of images in 3D electron microscopy and related fields. J. Struct. Biol. *116(1)*, 190–199.

Franke, D., Svergun, D.I. (2009). DAMMIF, a program for rapid ab-initio shape determination in small-angle scattering. J. Appl. Crystallogr. *42*, 342-346.

Gouet, P., Robert, X. and Courcelle, E. (2003). ESPript/ENDscirpt: extracting and rendering sequence and 3D information from atomic structures of proteins. Nucleic Acids Res. *31*, 3320–3323.

Humphrey, W., Dalke, A. and Schulten, K. (1996). VMD - Visual Molecular Dynamics. J. Mol. Graphics *14*, 33-38.

Kuwamoto, S., Akiyama, S., and Fujisawa, T. (2004). Radiation damage to a protein solution, detected by synchrotron X-ray small-angle scattering: dose-related considerations and suppression by cryoprotectants. J. Synchrotron Radiat. *11*, 462-468.

Langer, G., Cohen, S.X., Lamzin, V.S., and Perrakis, A. (2008). Automated macromolecular model building for X-ray crystallography using ARP/wARP version 7. Nat Protoc *3*, 1171-1179.

Larkin, M.A., Blackshields, G., Brown, N.P., Chenna, R., McGettigan, P.A., McWilliam, H., Valentin, F., Wallace, I.M., Wilm, A., Lopez, R., Thompson, J.D., Gibson, T.J. and Higgins, D.G. (2007). ClustalW and ClustalX version2. Bioinformatics, *23*, 2947–2948.

Ludtke, Steven J., Philip R. Baldwin, and Wah Chiu. (1999) EMAN: semiautomated software for high-resolution single-particle reconstructions. J. Struct. Biol. *128*, 82-97.

McPhillips, T. M., McPhillips, S. E., Chiu, H.-J., Cohen, A. E., Deacon, A. M., Ellis, P. J., Garman, E., et al. (2002). Blu-Ice and the Distributed Control System: software for data acquisition and instrument control at macromolecular crystallography beamlines. J. Synchrotron Radiat. *9*, 401–406.

Minor, W., Cymborowski, M., Otwinowski, Z., and Chruszcz, M. (2006). HKL-3000: the integration of data reduction and structure solution--from diffraction images to an initial model in minutes. Acta Crystallogr. D Biol. Crystallogr. *62*, 859-866.

Morris, R.J., Perrakis, A., and Lamzin, V.S. (2003). ARP/wARP and automatic interpretation of protein electron density maps. Methods in enzymology *374*, 229-244.

Murshudov, G.N., Vagin, A.A., and Dodson, E.J. (1997). Refinement of macromolecular structures by the maximum-likelihood method. Acta Crystallogr. D Biol. Crystallogr. *53*, 240-255.

Pettersen, E.F., Goddard, T.D., Huang, C.C., Couch, G.S., Greenblatt, D.M., Meng, E.C., and Ferrin, T.E. (2004). UCSF Chimera--a visualization system for exploratory research and analysis. J. Comput. Chem. *25*, 1605-1612.

Potterton, E., Briggs, P., Turkenburg, M., and Dodson, E. (2003). A graphical user interface to the CCP4 program suite. Acta Crystallogr. D Biol. Crystallogr. *59*, 1131-1137.

Russel, D., Lasker, K., Webb, B., Velázquez-Muriel, J., Tjioe, E., Schneidman-Duhovny, D., Peterson, B., and Sali, A. (2012). Putting the pieces together: integrative modeling platform software for structure determination of macromolecular assemblies. PLoS biology *10(1)*, e1001244.

Svergun, D.I. (1999). Restoring low resolution structure of biological macromolecules from solution scattering using simulated annealing. Biophysical J. *76*, 2879-2886

Terwilliger, T.C., Adams, P.D., Read, R.J., McCoy, A.J., Moriarty, N.W., Grosse-Kunstleve, R.W., Afonine, P.V., Zwart, P.H., and Hung, L.W. (2009). Decision-making in structure solution using Bayesian estimates of map quality: the PHENIX AutoSol wizard. Acta Crystallogr. D Biol. Crystallogr. *65*, 582-601.

Terwilliger, T.C., Grosse-Kunstleve, R.W., Afonine, P.V., Moriarty, N.W., Zwart, P.H., Hung, L.W., Read, R.J., and Adams, P.D. (2008). Iterative model building, structure refinement and density modification with the PHENIX AutoBuild wizard. Acta Crystallogr. D Biol. Crystallogr. *64*, 61-69.

Timney, B. L., Tetenbaum-Novatt, J., Agate, D. S., Williams, R., Zhang, W., Chait, B. T., and Rout, M. P. (2006). Simple kinetic relationships and nonspecific competition govern nuclear import rates in vivo. J. Cell Biol. *175*, 579-593.

Van Duyne, G.D., Standaert, R.F., Karplus, P.A., Schreiber, S.L., and Clardy, J. (1993). Atomic structures of the human immunophilin FKBP-12 complexes with FK506 and rapamycin. J. Mol. Biol. *229*, 105-124.

Velázquez-Muriel, J., Lasker, K., Russel, D., Phillips, J., Webb, B. M., Schneidman-Duhovny, D., and Sali, A. (2012). Assembly of macromolecular complexes by satisfaction of spatial restraints from electron microscopy images. Proc. Natl. Acad. Sci. USA. *109*, 18821-18826.

Volkov, V.V., Svergun, D. I. (2003). Uniqueness of ab initio shape determination in small-angle scattering. J. Appl. Crystallogr. *36*, 860-864.

Winn, M.D., Ballard, C.C., Cowtan, K.D., Dodson, E.J., Emsley, P., Evans, P.R., Keegan, R.M., Krissinel, E.B., Leslie, A.G., McCoy, A., *et al.* (2011). Overview of the CCP4 suite and current developments. Acta Crystallogr. D Biol. Crystallogr. *67*, 235-242.

Yang, Z., Fang, J., Chittuluru, J., Asturias, F. J., and Penczek, P. A. (2012). Iterative stable alignment and clustering of 2D transmission electron microscope images. Structure *20(2)*, 237-247.

Zenklusen, D., Wells, A. L., Condeelis, J. S., & Singer, R. H. (2007). Imaging real-time gene expression in living yeast. Cold Spring Harbor Protocols, *2007(11)*, pdb-prot4870.

Zhang, K.Y., Cowtan, K., and Main, P. (1997). Combining constraints for electron-density modification. Methods in Enzymology *277*, 53-64.

Zwart, P.H., Afonine, P.V., Grosse-Kunstleve, R.W., Hung, L.W., Ioerger, T.R., McCoy, A.J., McKee, E., Moriarty, N.W., Read, R.J., Sacchettini, J.C., *et al.* (2008). Automated structure solution with the PHENIX suite. Methods in Mol. Biol. *426*, 419-435.